Pulsed EM field transfer between a horizontal electric dipole and a transmission line
A closed-form model based on the Cagniard-DeHoop technique

Stumpf, Martin; Antonini, Giulio ; Lager, Ioan E.

DOI
10.1109/TAP.2019.2935115

Publication date
2020

Document Version
Accepted author manuscript

Published in
IEEE Transactions on Antennas and Propagation

Pulsed EM Field Transfer Between a Horizontal Electric Dipole and a Transmission Line – A Closed-Form Model Based on the Cagniard-DeHoop Technique

Martin Štumpf, *Member, IEEE*, Giulio Antonini, *Senior Member, IEEE*, and Ioan E. Lager, *Senior Member, IEEE*

***Abstract*—The pulsed electromagnetic (EM) field transfer between a horizontal electric dipole (HED) and a transmission line is described analytically with the aid of the time-domain (TD) reciprocity theorem and the Cagniard-DeHoop technique. It is demonstrated that a suitably chosen wave-slowness representation makes it possible to cast the pertaining interaction integrals into a form amenable to analytical solution. The closed-form coupling model thus obtained clearly reveals the dependence of configurational parameters on the wireless signal transfer. Numerical results are presented and validated using a three-dimensional EM computational tool.**

***Index Terms*—time-domain analysis, Cagniard-DeHoop method, electromagnetic scattering, electromagnetic coupling, transmission lines;**

I. Introduction

THE constant need for still higher data rates in the increasingly congested radio spectrum has triggered the intensive research into the pulsed EM transfer which is deemed to be a promising enabler for designing inter- and intra-chip wireless interconnects in integrated circuit devices [1], [2], [3] and ultra-high data-rate, safe and reliable digital communication systems [4], [5], [6]. A wireless interconnect system, in general, consists of transmitting and receiving antennas that are mutually coupled via the radiative EM coupling path. Whenever the pulse-time width of an excitation pulse is large enough such that the EM field surrounding the conductor of a receiving antenna has the transverse EM structure, the transmission-line theory [7] can be employed to capture the dominant coupling mechanism in the pulsed EM transfer. To that end, a number of EM-field-to-transmission-line coupling models have been proposed (see [8], [9]), successfully validated (e.g. [10], [11]) and applied to antenna-to-transmission line coupling problems (e.g. [12], [13]) and EM-field susceptibility studies (e.g. [14], [15]).

While the relevant analytical models in the frequency domain (FD) are capable of analyzing relatively complex problems including radiation and dissipation phenomena [16], [17], the corresponding TD developments are mostly limited to loss-free transmission lines on a (piecewise-)homogeneous background excited by a uniform EM plane wave (e.g. [18], [14]). For describing the transfer of EM pulses radiated from spatially localized EM sources such as a CMOS integrated-loop antenna [19], [20] or a lightning return stroke [15], however, the plane-wave coupling models are no longer practical. Accordingly, having the limitation in mind, Ref. [21] introduced closed-form expressions describing the TD voltages on a transmission line excited by a vertical electric dipole (VED), which proved to be efficient for lightning-induced voltage calculations [22]. Moreover, such a closed-form EM coupling model clearly indicates the relevant excitation and configurational parameters, thus making it possible to optimize the pertaining signal transfer (e.g. [23]) with very low computational efforts that are virtually independent of the relative source-field distance. In contrast to the excitation EM fields radiated from a VED source above a planar interface, the corresponding fields radiated from a HED source are generally composed of both TE- and TM-type waves [24, Sec. 2.3]. As a consequence, the methodology applied in the previous works [21], [22] is not directly applicable to the actual problem, which calls for a new solution strategy. Introducing such a Cagniard-DeHoop-based methodology [25], [26] that yields a novel analytical description of the pulsed EM transfer between a HED and a transmission line is exactly the main purpose of the present paper.

The problem under consideration is formulated in Sec. II using the EM reciprocity theorem of the time-convolution type (see [27, Sec. 28.2] and [28, Sec. 1.4.1]). In the following Sec. III, the EM fields radiated from a HED source above a perfect ground are expressed via wave-slowness representations. Here, the slowness representation of the horizontal component of the excitation field is cast into the form that enables to integrate the field along the line analytically. In this manner, we find complex-FD expressions for the

M. Štumpf is with the Department of Radioelectronics, Brno University of Technology, Technická 3082/12, 616 00 Brno, The Czech Republic (e-mail: martin.stumpf@centrum.cz).

G. Antonini is with the UAq EMC Laboratory, University of L'Aquila, 67 100 L'Aquila, Italy (e-mail: giulio.antonini@univaq.it).

I. E. Lager is with the Faculty of Electrical Engineering, Mathematics and Computer Science, Delft University of Technology, Delft 2628 CD, the Netherlands (e-mail: i.e.lager@tudelft.nl).

Manuscript received April 26, 2019; revised July 17, 2019; accepted August 05, 2019. The research reported in this paper was carried out during a visiting professorship M. Štumpf had effectuated at the UAq EMC Laboratory, University of L'Aquila, Italy. The research was financially supported by the Czech Ministry of Education, Youth and Sports under Grant LO1401, which is gratefully acknowledged.

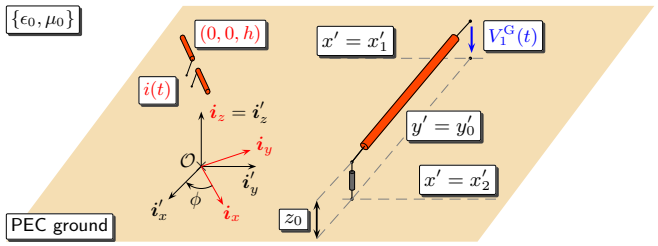

Fig. 1. A transmission line excited by an impulsive horizontal electric dipole.

induced-voltage response that are amenable to the Cagniard-DeHoop method. The resulting analytical TD expressions for the HED-induced Thévenin's voltages on a transmission line are given in Sec. IV. The latter section heavily relies on the Appendix, where the corresponding Cagniard-DeHoop technique is closely described on the transformation of generic constituents. In Sec. V, illustrative numerical examples are presented and validated using a three-dimensional EM computational tool. Finally, conclusions are drawn and potential applications are hinted at in Sec. VI.

II. Problem Description

We shall analyze the TD voltage response of a transmission line induced by an elementary HED (see Fig. 1). Position in the problem configuration is specified by the Cartesian coordinates $\{x, y, z\}$ with respect to a Cartesian reference frame with the origin $\mathcal{O}$ and the standard base $\{\boldsymbol{i}_x, \boldsymbol{i}_y, \boldsymbol{i}_z\}$. The time coordinate is $t > 0$ and the time-convolution operator is denoted by $*_t$. The Dirac-delta distribution is denoted by $\delta(t)$ and the Heaviside-unit step function is $\mathrm{H}(t)$. The partial differentiation is denoted by ∂ that is supplied with the pertaining subscript.

Without loss of generality, the exciting HED is oriented along the x-direction and is located at $(0, 0, h > 0)$ above the unbounded, planar and perfectly electrically conducting (PEC) ground plane in a homogeneous, isotropic and loss-free half-space $z > 0$. The EM properties of the half-space are described by its (real-valued, scalar and positive) electric permittivity ϵ_0 and magnetic permeability μ_0. The corresponding EM wave speed is $c_0 = (\epsilon_0\mu_0)^{-1/2} > 0$ and the wave impedance is denoted by $\zeta_0 = (\mu_0/\epsilon_0)^{1/2} > 0$. The source signature is described by $j(t) = i(t)\Delta x$ (in $\mathrm{A}\cdot\mathrm{m}$), where $i(t)$ is the electric-current pulse and $\Delta x > 0$ denotes the (short) dipole's length. It is further assumed that the source starts to radiate at $t = 0$ and prior to this instant EM fields are zero throughout the problem configuration.

The transmission line under consideration is made of PEC and is located along $\{x'_1 < x' < x'_2, y' = y'_0, z' = z_0\}$ with respect to a rotated Cartesian coordinate system with coordinates $\{x', y', z'\}$ defined by

$$x' = x\cos(\phi) + y\sin(\phi) \tag{1}$$
$$y' = -x\sin(\phi) + y\cos(\phi) \tag{2}$$
$$z' = z \tag{3}$$

where $\{0 \leq \phi < 2\pi\}$ is the angle of rotation (see Fig. 1). The transmission line's end points at $\{x_{1,2}, y_{1,2}, z_0\}$ then simply correspond to $\{x'_{1,2}, y'_0, z_0\}$ in the rotated coordinate system, respectively. The length of the transmission line is denoted by $L = x'_2 - x'_1$.

The problem is formulated with the aid of the EM reciprocity theorem of the time-convolution type (see [27, Sec. 28.2] and [28, Sec. 1.4.1]) along the lines proposed in Ref. [29]. Through the reciprocity theorem, the (actual) receiving (R) situation is interrelated with the (auxiliary) testing (T) state in which the transmission line operates as a transmitter. This way yields (cf. [29, Eq. (7)] and [22, Eq. (1)])

$$\begin{aligned} &V_1^{\mathrm{R}}(t) *_t I_1^{\mathrm{T}}(t) - V_1^{\mathrm{T}}(t) *_t I_1^{\mathrm{R}}(t) \\ &\quad - V_2^{\mathrm{R}}(t) *_t I_2^{\mathrm{T}}(t) + V_2^{\mathrm{T}}(t) *_t I_2^{\mathrm{R}}(t) \\ &\simeq -\int_{x'=x'_1}^{x'_2} E^{\mathrm{e}}_{x'}(x', y'_0, z_0, t) *_t I^{\mathrm{T}}(x', t)\mathrm{d}x' \\ &\quad - I_1^{\mathrm{T}}(t) *_t \int_{z=0}^{z_0} E^{\mathrm{e}}_z(x_1, y_1, z, t)\mathrm{d}z \\ &\quad + I_2^{\mathrm{T}}(t) *_t \int_{z=0}^{z_0} E^{\mathrm{e}}_z(x_2, y_2, z, t)\mathrm{d}z \end{aligned} \tag{4}$$

where the relevant voltage and electric-current quantities at $x' = x'_{1,2}$ are denoted by $\{V_{1,2}, I_{1,2}\}$, respectively, and superscript (e) denotes the excitation field, that is, the total EM field radiated from the HED source located above the ground plane in the absence of the transmission line. Accordingly, the left-hand side of the reciprocity relation (4) can be interpreted as a TD interaction of the terminal voltages and currents, while the right-hand side represents the weighted contribution of the excitation-field distribution along the transmission line. If the transmission line is at $x' = x'_2$ matched in both (R) and (T) states and excited via the electric-current Dirac-impulse source at $x' = x'_1$ in state (T), i.e. $I_1^{\mathrm{T}}(t) = \delta(t)$, Eq. (4) has the following form (cf. [29, Eq. (47)])

$$\begin{aligned} V_1^{\mathrm{G}}(t) \simeq &-\int_{x'=x'_1}^{x'_2} E^{\mathrm{e}}_{x'}[x', y'_0, z_0, t - (x' - x'_1)/c_0]\mathrm{d}x' \\ &- \int_{z=0}^{z_0} E^{\mathrm{e}}_z(x_1, y_1, z, t)\mathrm{d}z \\ &+ \int_{z=0}^{z_0} E^{\mathrm{e}}_z(x_2, y_2, z, t - L/c_0)\mathrm{d}z \end{aligned} \tag{5}$$

where $V_1^{\mathrm{G}}(t)$ is the open-circuited (Thévenin's) voltage observed at $x' = x'_1$. A similar procedure leads to the Thévenin-voltage expression at the far-end of the transmission line, that is

$$\begin{aligned} V_2^{\mathrm{G}}(t) \simeq &\int_{x'=x'_1}^{x'_2} E^{\mathrm{e}}_{x'}[x', y'_0, z_0, t - (x'_2 - x')/c_0]\mathrm{d}x' \\ &- \int_{z=0}^{z_0} E^{\mathrm{e}}_z(x_2, y_2, z, t)\mathrm{d}z \\ &+ \int_{z=0}^{z_0} E^{\mathrm{e}}_z(x_1, y_1, z, t - L/c_0)\mathrm{d}z \end{aligned} \tag{6}$$

The right-hand sides of Eqs. (5)–(6) will next be evaluated via the Cagniard-DeHoop method [25], thereby yielding the TD impedance transfer functions describing the pulsed EM-field signal transfer, $V_{1,2}^{\mathrm{G}}(t) = \mathcal{Z}_{1,2}(x'_1, x'_2, y'_0, z_0, h, \phi, t) *_t i(t)$, respectively (see Fig. 1).

III. Slowness-Domain Representation of Excitation Fields

The time invariance of the problem configuration and the causality of the excited EM waves are properly accounted for via the one-sided Laplace transformation. To show the notation, the expression is given for the x-component of the excitation electric-field strength, that is

$$\hat{E}^{\mathrm{e}}_x(x,y,z,s)=\int_{t=0}^{\infty}\exp(-st)E^{\mathrm{e}}_x(x,y,z,t)\mathrm{d}t \tag{7}$$

with $\{s\in\mathbb{R};s>0\}$ thus relying on Lerch's uniqueness theorem [28, Appendix]. The Cagniard-DeHoop technique combines the Laplace transformation (7) with the wave-slowness representation

$$\begin{aligned}\hat{E}^{\mathrm{e}}_x(x,y,z,s)&=(s/2\pi\mathrm{i})^2\int_{\kappa=-\mathrm{i}\infty}^{\mathrm{i}\infty}\mathrm{d}\kappa\\&\times\int_{\sigma=-\mathrm{i}\infty}^{\mathrm{i}\infty}\exp[-s(\kappa x+\sigma y)]\tilde{E}^{\mathrm{e}}_x(\kappa,\sigma,z,s)\mathrm{d}\sigma\end{aligned} \tag{8}$$

where κ and σ are slowness parameters in the x- and y-direction, respectively. Under the slowness representation, the electric-field strength radiated from a HED source above the perfect ground plane can be expressed as

$$\begin{aligned}\tilde{E}^{\mathrm{e}}_{x'}(\kappa,\sigma,z,s)&=-\zeta_0 s\hat{j}(s)c_0^{-1}\tilde{G}(\kappa,\sigma,z,s)\cos(\phi)\\&+\zeta_0 s\hat{j}(s)c_0\kappa[\kappa\cos(\phi)+\sigma\sin(\phi)]\tilde{G}(\kappa,\sigma,z,s)\end{aligned} \tag{9}$$

$$\tilde{E}^{\mathrm{e}}_z(\kappa,\sigma,z,s)=-\zeta_0\hat{j}(s)c_0\kappa\partial_z\tilde{G}(\kappa,\sigma,z,s) \tag{10}$$

in which $\tilde{G}$ is the transform-domain Green's function representing the one-dimensional wave motion emanating from the point source and its image accounting for the presence of the ground plane at $z=0$. Accordingly, the Green's function reads

$$\begin{aligned}\tilde{G}(\kappa,\sigma,z,s)&=\exp[-s\gamma_0|z-h|]/2s\gamma_0\\&-\exp[-s\gamma_0(z+h)]/2s\gamma_0\end{aligned} \tag{11}$$

for all $z\geq 0$, where $\gamma_0=\gamma_0(\kappa,\sigma)=[\Omega_0^2(\kappa)-\sigma^2]^{1/2}=(c_0^{-2}-\kappa^2-\sigma^2)^{1/2}$ with $\mathrm{Re}(\gamma_0)>0$. The form of the source-type transform-domain representation of the horizontal excitation-field component (9) suggests to transform the wave slowness parameters according to (cf. Eqs. (1)–(2))

$$\kappa=v\cos(\phi)-p\sin(\phi) \tag{12}$$

$$\sigma=v\sin(\phi)+p\cos(\phi) \tag{13}$$

Under this transformation $\kappa^2+\sigma^2=v^2+p^2$, $\kappa x+\sigma y=vx'+py'$ and $\mathrm{d}\kappa\mathrm{d}\sigma=\mathrm{d}v\mathrm{d}p$. Subsequently, subject to (12)–(13), Eq. (8) transforms to

$$\begin{aligned}\hat{E}^{\mathrm{e}}_x(x,y,z,s)&=(s/2\pi\mathrm{i})^2\int_{v=-\mathrm{i}\infty}^{\mathrm{i}\infty}\mathrm{d}v\\&\times\int_{p=-\mathrm{i}\infty}^{\mathrm{i}\infty}\exp[-s(vx'+py')]\bar{E}^{\mathrm{e}}_x(v,p,z,s)\mathrm{d}p\end{aligned} \tag{14}$$

and, finally, Eq. (9) transforms to

$$\begin{aligned}\bar{E}^{\mathrm{e}}_{x'}(v,p,z,s)&=-\zeta_0 s\hat{j}(s)c_0\Omega_0^2(v)\tilde{G}(v,p,z,s)\cos(\phi)\\&-\zeta_0 s\hat{j}(s)c_0 vp\,\tilde{G}(v,p,z,s)\sin(\phi)\end{aligned} \tag{15}$$

where we used $\Omega_0(v)=(c_0^{-2}-v^2)^{1/2}>0$.

IV. Time-Domain Thévenin's Voltage Responses

The wave-slowness representations derived in the previous section are next used to construct space-time expressions for the induced Thévenin's voltage responses (see Eqs. (5)–(6) and Fig. 1). The contributions from the horizontal (with respect to the ground plane) component of the excitation field, say $V^{\mathrm{G};\parallel}_{1,2}(t)$ and from the vertical one denoted by $V^{\mathrm{G};\perp}_{1,2}(t)$ will be discussed separately. The total voltage response then follows as

$$V^{\mathrm{G}}_{1,2}(t)=V^{\mathrm{G};\parallel}_{1,2}(t)+V^{\mathrm{G};\perp}_{1,2}(t) \tag{16}$$

for all $t>0$.

A. Horizontal excitation-field contributions

The transform-domain expression for the horizontal component of the excitation field (15) is used in the slowness representation (14), where the dependence on the axial coordinate x' manifests itself through the exponential function only. Consequently, the spatial integration with respect to x' (see Eqs. (5)–(6)) is elementary, which yields an s-domain expression that is amenable to the Cagniard-DeHoop methodology as specified in the Appendix. In this way, we arrive at

$$\begin{aligned}V^{\mathrm{G};\parallel}_1(t)&=-\zeta_0\partial_t j(t)*_t\Big\{[I(x_2',y_0',Z^{\mathrm{i}},t-L/c_0)\\&-I(x_1',y_0',Z^{\mathrm{i}},t)]\cos(\phi)-[I(x_2',y_0',Z^{\mathrm{r}},t-L/c_0)\\&-I(x_1',y_0',Z^{\mathrm{r}},t)]\cos(\phi)+[J(x_2',y_0',Z^{\mathrm{i}},t-L/c_0)\\&-J(x_1',y_0',Z^{\mathrm{i}},t)]\sin(\phi)-[J(x_2',y_0',Z^{\mathrm{r}},t-L/c_0)\\&-J(x_1',y_0',Z^{\mathrm{r}},t)]\sin(\phi)\Big\}\end{aligned} \tag{17}$$

where $Z^{\mathrm{i}}=|z_0-h|$, $Z^{\mathrm{r}}=z_0+h$ and space-time functions $I(x,y,z,t)$ with $J(x,y,z,t)$ are given by Eqs. (34) and (36), respectively, in the Appendix. Upon inspection of Eqs. (5)–(6), the corresponding contribution at $x'=x_2'$ follows

$$\begin{aligned}V^{\mathrm{G};\parallel}_2(t)&=\zeta_0\partial_t j(t)*_t\Big\{[I(-x_1',y_0',Z^{\mathrm{i}},t-L/c_0)\\&-I(-x_2',y_0',Z^{\mathrm{i}},t)]\cos(\phi)-[I(-x_1',y_0',Z^{\mathrm{r}},t-L/c_0)\\&-I(-x_2',y_0',Z^{\mathrm{r}},t)]\cos(\phi)-[J(-x_1',y_0',Z^{\mathrm{i}},t-L/c_0)\\&-J(-x_2',y_0',Z^{\mathrm{i}},t)]\sin(\phi)+[J(-x_1',y_0',Z^{\mathrm{r}},t-L/c_0)\\&-J(-x_2',y_0',Z^{\mathrm{r}},t)]\sin(\phi)\Big\}\end{aligned} \tag{18}$$

Finally, Eqs. (17)–(18) are substituted in Eq. (16) to get the total voltage response.

B. Vertical excitation-field contributions

The transform-domain expression for the vertical component of the excitation field (10) is integrated with respect to z (see Eqs. (5)–(6)) and the result of integration is substituted in the slowness representation of type (8). This procedure leads to an expression in the s-domain that can be transformed back to the original domain as described in Sec. C of the Appendix. Following these lines, we end up with

$$\begin{aligned}V^{\mathrm{G};\perp}_1(t)&=\zeta_0\partial_t j(t)*_t\Big\{K(x_1,y_1,Z^{\mathrm{i}},t)\\&-K(x_1,y_1,Z^{\mathrm{r}},t)-K(x_2,y_2,Z^{\mathrm{i}},t-L/c_0)\\&+K(x_2,y_2,Z^{\mathrm{r}},t-L/c_0)\Big\}\end{aligned} \tag{19}$$

where space-time function $K(x,y,z,t)$ is given by Eq. (39). Upon inspection of Eqs. (5)–(6), we find

$$V_2^{\mathrm{G};\perp}(t) = \zeta_0 \partial_t j(t) *_t \Big\{ K(x_2, y_2, Z^{\mathrm{i}}, t) - K(x_2, y_2, Z^{\mathrm{r}}, t) - K(x_1, y_1, Z^{\mathrm{i}}, t - L/c_0) + K(x_1, y_1, Z^{\mathrm{r}}, t - L/c_0) \Big\} \tag{20}$$

Finally, Eqs. (19)–(20) are substituted in Eq. (16) to get the total voltage response.

V. Illustrative Numerical Examples

In this section, a number of illustrative problem configurations are analyzed. Namely, we shall calculate the voltage response of a transmission line of a length $L = 100\,\mathrm{mm}$ that is located at a height $z_0 = L/25$ above the perfect ground plane. The transmission line is excited by a HED of a length $\mathrm{d}x = L/100$ that is placed above the origin at a height $h = 3L/20$. The transmitting antenna is activated by a causal electric-current pulse with finite temporal support that can be simply constructed by convolving a triangular pulse with a rectangular one. Accordingly, the input electric-current pulse is described by

$$i(t) = i_{\mathrm{m}} \Bigg[2\left(\frac{t}{t_{\mathrm{w}}}\right)^2 \mathrm{H}(t) - 4\left(\frac{t}{t_{\mathrm{w}}} - \frac{1}{2}\right)^2 \mathrm{H}\left(\frac{t}{t_{\mathrm{w}}} - \frac{1}{2}\right) + 4\left(\frac{t}{t_{\mathrm{w}}} - \frac{3}{2}\right)^2 \mathrm{H}\left(\frac{t}{t_{\mathrm{w}}} - \frac{3}{2}\right) - 2\left(\frac{t}{t_{\mathrm{w}}} - 2\right)^2 \mathrm{H}\left(\frac{t}{t_{\mathrm{w}}} - 2\right) \Bigg] \tag{21}$$

where we take $i_{\mathrm{m}} = 1.0\,\mathrm{A}$ and $c_0 t_{\mathrm{w}} = 5L$ (see Fig. 2). Hence, the length of the HED and the height of the transmission line are relatively small with respect to the spatial support of the current pulse, namely, $\mathrm{d}x/c_0 t_{\mathrm{w}} = 1/500$ and $z_0/c_0 t_{\mathrm{w}} = 1/125$, thereby meeting the assumptions made for the coupling model to apply. For the sake of validation, the problem is also analyzed using the finite integration technique (FIT) as implemented in CST Microwave Studio®. Here, the line is represented by a circular cylinder of a radius $r = L/100$. The characteristic impedance matching the line then follows as $Z^{\mathrm{c}} = (\zeta_0/2\pi)\cosh^{-1}(z_0/r) \simeq 124\,\Omega$ [11].

The chosen configurational parameters for the first example $x_1' = -L/2$, $x_2' = L/2$, $y_0' = 3L/4$ and $\phi = 0$ imply that the exciting HED is oriented in parallel with respect to the transmission line and is equidistant from its terminals (see Fig. 3a). From Eqs. (17)–(18) it is clearly seen that for $\phi = 0$ and $x_1' = -x_2'$ we have $V_1^{\mathrm{G};\parallel}(t) = -V_2^{\mathrm{G};\parallel}(t)$. Since $K(x,y,z,t)$ as given by Eq. (39) is an odd function of x, we also have $V_1^{\mathrm{G};\perp}(t) = -V_2^{\mathrm{G};\perp}(t)$ and hence $V_1^{\mathrm{G}}(t) = -V_2^{\mathrm{G}}(t)$ in total as observed in Fig. 3b. The discrepancies with respect to the voltage pulses calculated via the FIT are acceptable and can be largely attributed to the simplifying assumptions of the analytical model and to numerical errors. Finally, it is interesting to note that the calculated voltage pulses have approximately the shape of a bipolar triangle, which is, in fact, the shape of $\partial_t i(t)$ (see Eq. (21)).

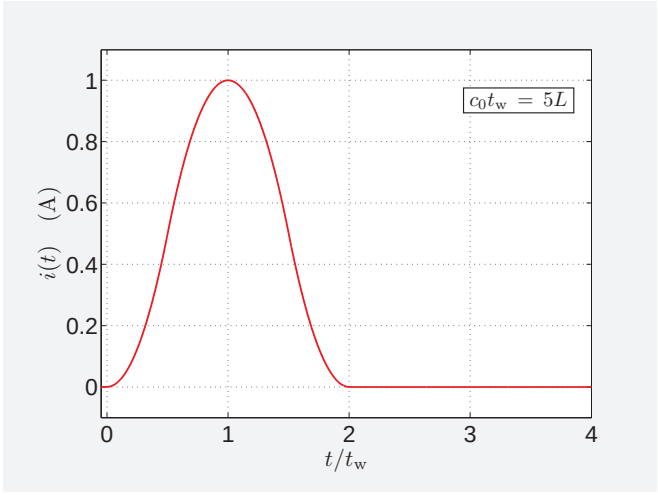

Fig. 2. Excitation electric-current pulse shape.

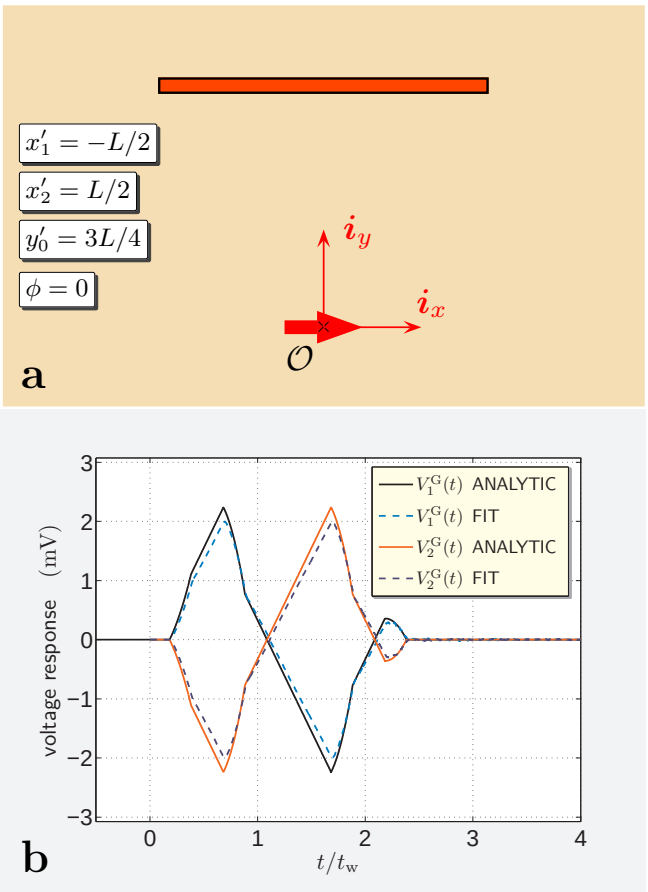

Fig. 3. (a) Top view of the problem configuration; (b) HED-induced Thévenin-voltage responses.

In the second example, the line is horizontally shifted with respect to the source by changing $\{x_1', x_2'\}$ to $x_1' = -L/4$ and $x_2' = 3L/4$ (see Fig. 4a). In this case, the distance from the source to the transmission-line terminals is not equal anymore, which manifests itself by the time shift between the pulse shapes shown in Fig. 4b. While the voltage pulse observed at the far-end terminal still starts with a negative lobe, its

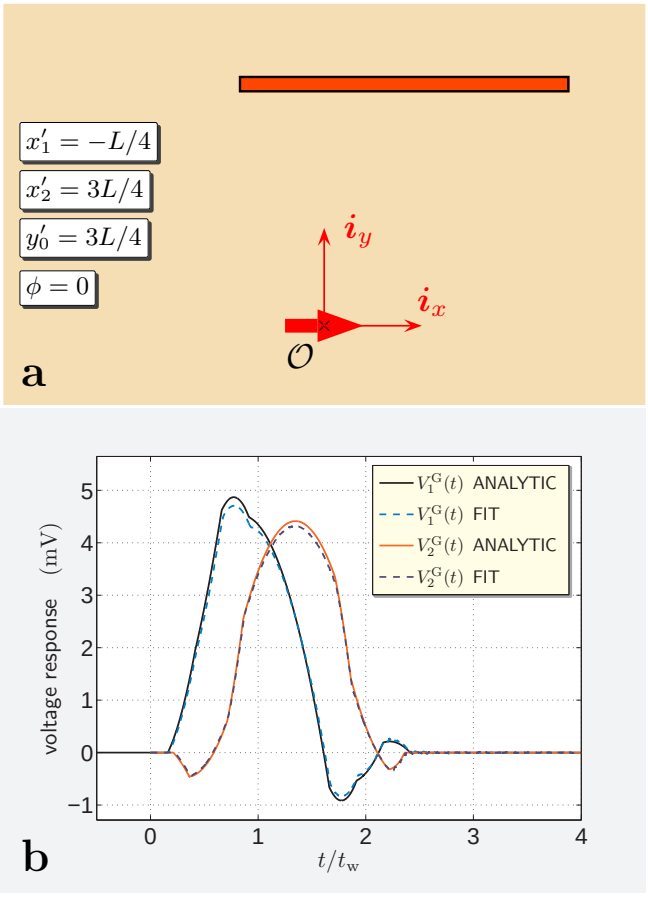

Fig. 4. (a) Top view of the problem configuration; (b) HED-induced Thévenin-voltage responses.

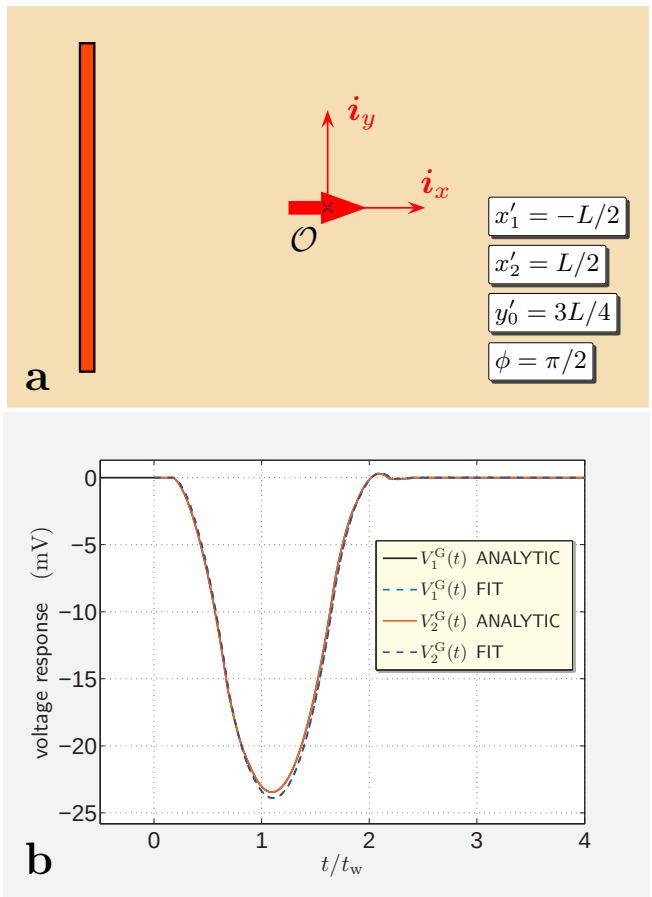

Fig. 5. (a) Top view of the problem configuration; (b) HED-induced Thévenin-voltage responses.

shape is now more similar to the scaled copy of the (unipolar) excitation electric-current pulse. The corresponding results calculated via the FIT agree well with the ones predicted by the analytical model.

For $x_1' = -x_2'$ and $\phi = \pi/2$, Eqs. (17)–(18) reveal that $V_1^{G;\parallel}(t) = V_2^{G;\parallel}(t)$ in the third example (see Fig. 5a). Also, since $x_1 = x_2 = -y_0' = -3L/4$ and $y_1 = x_1' = -L/2 = -y_2$ together with the property $K(x, y, z, t) = K(x, -y, z, t)$ (see Eqs. (19)–(20) with (39)) we have $V_1^{G;\perp}(t) = V_2^{G;\perp}(t)$, which yields $V_1^G(t) = V_2^G(t)$ in total. Hence, the calculated voltage pulses at the transmission-line terminals are identical in this case (see Fig. 5b). Clearly, their shape resemble the negative scaled copy of the excitation pulse, which has also been confirmed with the aid of FIT.

Finally, the transmission line has been rotated by $\phi = \pi/12$ with respect to the axis of the exciting HED. Similarly to the second example, its position in the rotated coordinate system is determined by $x_1' = -L/4$, $x_2' = 3L/4$ and $y_0' = 3L/4$ (see Fig. 6a). Figure 6b then demonstrates that the excitation electric-current pulse is heavily distorted upon traversing the distance to the receiving transmission-line terminals. The correspondence with the pulses calculated using the FIT is satisfactory again.

VI. Conclusions

A closed-form TD coupling model describing the pulsed EM-field signal transfer between an impulsive HED source and a transmission line has been constructed via the Cagniard-DeHoop technique. As the influence of configurational parameters on the signal transfer clearly shows up in the analytical and easy-to-implement formulas, they lend themselves to their application in solving multi-objective optimization tasks aiming at distortion-free or/and energy-effective EM pulse transfers. Illustrative numerical examples demonstrated the intricate distortion undergone by the exciting electric-current pulse on its way from the HED source to the receiving ports of a transmission line as well as the validity of the model. Since the computational burden of direct-discretization techniques (e.g. the finite-difference TD technique) increases rapidly with the growing solution domain, the computational resources required by such numerical techniques are exceedingly high whenever the transmission line is relatively far away from its exciting source. In such cases, the derived closed-form formulas, whose computational effort is virtually independent of the mutual HED-to-transmission-line distance, can provide useful approximate results. Thanks to the problem linearity, the sum of contributions due to a collection of HEDs can serve for representing the voltage response induced by a small, conducting, current-carrying thin wire in the shape

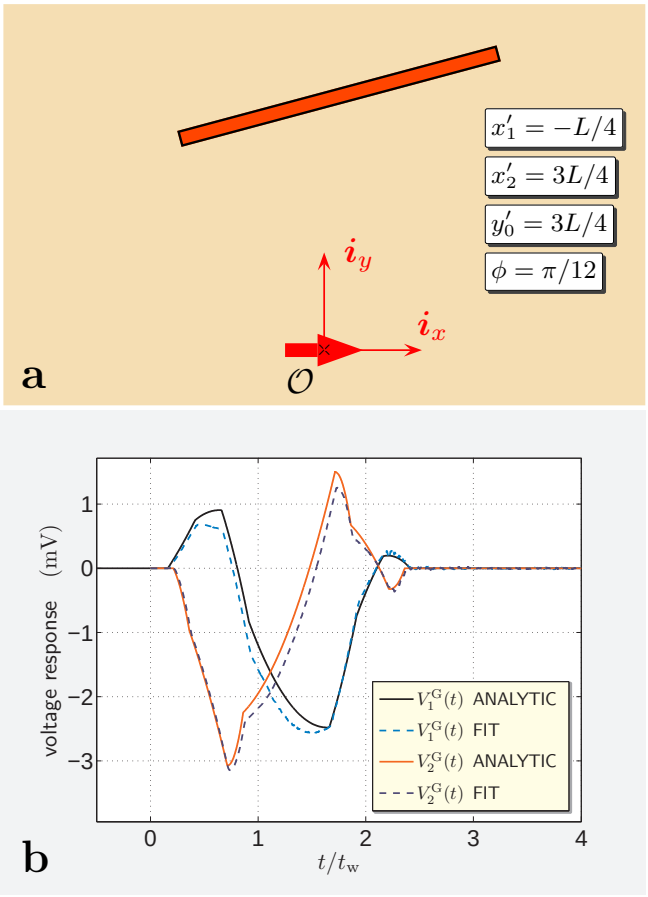

Fig. 6. (a) Top view of the problem configuration; (b) HED-induced Thévenin-voltage responses.

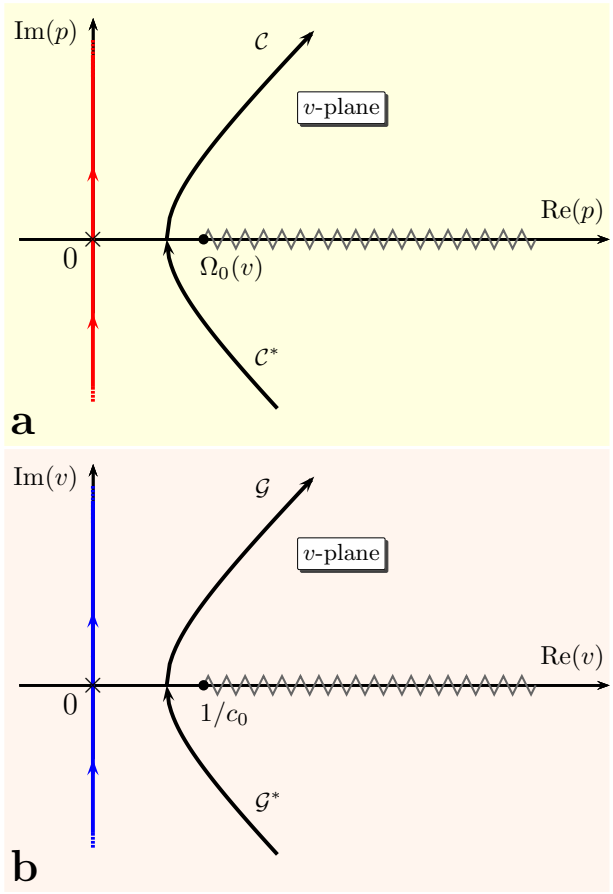

Fig. 7. Complex slowness planes. (a) p-plane with the Cagniard-DeHoop path for $y > 0$; (b) v-plane with the Cagniard-DeHoop path for $x > 0$.

of a loop, thereby yielding the pulsed EM field transfer between a vertical magnetic dipole and a transmission line [27, Sec. 26.10]. Moreover, the proposed coupling model can be further extended to analyze the crosstalk between two lines [30] and, in combination with the results presented in [22, Appendix], to obtain an efficient analytical model for analyzing the induced voltages on a transmission line due to a tortuous lightning channel [31].

APPENDIX

In this Appendix we shall derive the TD counterparts of generic integrals from which the HED-induced voltage on a transmission line can be constructed.

A. Space-time function $I(x, y, z, t)$

The first generic representation to be transformed to the TD has the following form

$$\hat{I}(x,y,z,s) = \frac{c_0}{8\pi^2 \mathrm{i}^2}\int_{v=-\mathrm{i}\infty}^{\mathrm{i}\infty} \exp(-svx)\frac{\Omega_0^2(v)}{v+c_0^{-1}}\mathrm{d}v \times \int_{p=-\mathrm{i}\infty}^{\mathrm{i}\infty} \exp\{-s[py+\gamma_0(v,p)z]\}\frac{\mathrm{d}p}{\gamma_0(v,p)} \quad (22)$$

for $x, y \in \mathbb{R}$, $\{z \in \mathbb{R}; z > 0\}$, $\{s \in \mathbb{R}; s > 0\}$ and recall that $\gamma_0 = \gamma_0(v,p) = [\Omega_0^2(v) - p^2]^{1/2} = (c_0^{-2} - v^2 - p^2)^{1/2}$ with $\mathrm{Re}(\gamma_0) > 0$. At first, the integrand with respect to p is analytically continued into the complex p-plane away from the imaginary axis and the integration path is in virtue of Jordan's lemma and Cauchy's theorem deformed into the hyperbolic Cagniard-DeHoop path defined by

$$py + \gamma_0(v,p)z = ud\,\Omega_0(v) \quad (23)$$

for $\{u \in \mathbb{R}; u \geq 1\}$ and $d = (y^2+z^2)^{1/2} > 0$. Upon solving Eq. (23) for p, we find path parametrization $\mathcal{C} \cup \mathcal{C}^*$ (* denotes the complex conjugate), where

$$\mathcal{C} = \Big\{p(u) = \big[(y/d)u + \mathrm{i}(z/d)(u^2-1)^{1/2}\big]\Omega_0(v)\Big\} \quad (24)$$

for all $\{1 \leq u < \infty\}$ (see Fig. 7a). Combining the contributions of integration from $\mathcal{C}$ and $\mathcal{C}^*$ and introducing the parameter u as the variable of integration with the Jacobian

$$\frac{\partial p}{\partial u} = \frac{\mathrm{i}\gamma_0[v,p(u)]}{(u^2-1)^{1/2}} \quad (25)$$

along $\mathcal{C}$, we obtain

$$\hat{I}(x,y,z,s) = \frac{c_0}{4\pi^2\mathrm{i}}\int_{u=1}^{\infty}\frac{\mathrm{d}u}{(u^2-1)^{1/2}} \times \int_{v=-\mathrm{i}\infty}^{\mathrm{i}\infty}\exp\{-s[vx+ud\,\Omega_0(v)]\}(c_0^{-1}-v)\mathrm{d}v \quad (26)$$

where we changed the order of the integrations. In the ensuing step, we proceed similarly in the complex v-plane. Hence, the integrand with respect to v is first continued analytically away from the imaginary axis and the integration contour along $\mathrm{Re}(v) = 0$ is replaced with the corresponding Cagniard-DeHoop path, whose parametrization is found from

$$vx + \Omega_0(v)\, ud = \tau \tag{27}$$

where $\{\tau \in \mathbb{R}; \tau > 0\}$. Solving Eq. (27) for v we obtain another hyperbolic-path parametrization $\mathcal{G} \cup \mathcal{G}^*$, with

$$\mathcal{G} = \Big\{ v(\tau) = \big\{ x\tau + \mathrm{i}ud[\tau^2 - R^2(u)/c_0^2]^{1/2} \big\}/R^2(u) \Big\} \tag{28}$$

for all $\{R(u)/c_0 \leq \tau < \infty\}$ with $R(u) = (x^2 + u^2 d^2)^{1/2} > 0$ (see Fig. 7b). Taking into account the symmetry of the Cagniard-DeHoop path with respect to $\mathrm{Im}(v) = 0$ and using

$$\frac{\partial v}{\partial \tau} = \frac{\mathrm{i}\Omega_0[v(\tau)]}{[\tau^2 - R^2(u)/c_0^2]^{1/2}} \tag{29}$$

to introduce τ as the variable of integration, we find

$$\begin{aligned} \hat{I}(x,y,z,s) &= \frac{c_0 d}{2\pi^2} \int_{u=1}^{\infty} \frac{u\mathrm{d}u}{R^2(u)(u^2-1)^{1/2}} \\ &\times \int_{\tau=R(u)/c_0}^{\infty} \exp(-s\tau) \Big[\tau/c_0 - 2x\tau^2/R^2(u) + x/c_0^2 \Big] \\ &\times [\tau^2 - R^2(u)/c_0^2]^{-1/2} \mathrm{d}\tau \end{aligned} \tag{30}$$

where we have explicitly specified the integrand along the Cagniard-DeHoop path. Interchanging further the order of the integrations, we arrive at

$$\begin{aligned} \hat{I}(x,y,z,s) &= (1/2\pi^2) \int_{\tau=R/c_0}^{\infty} \exp(-s\tau)\mathrm{d}\tau \\ &\times \int_{u=1}^{U(\tau)} R^{-2}(u) \Big[c_0\tau - 2xc_0^2\tau^2/R^2(u) + x \Big] \\ &\times (u^2-1)^{-1/2} [U^2(\tau) - u^2]^{-1/2} u\mathrm{d}u \end{aligned} \tag{31}$$

where $R = R(1) = (x^2 + y^2 + z^2)^{1/2}$ and $U(\tau) = (c_0^2\tau^2 - x^2)^{1/2}/d > 0$. The integrand with respect to u shows the inverse square-root singularities at the end points of integration that are handled via [32, Appendix A]

$$u^2 = \cos^2(\psi) + U^2(\tau)\sin^2(\psi) \tag{32}$$

for $\{0 \leq \psi \leq \pi/2\}$. Under the substitution, the integral with respect to u can be readily carried out analytically and we end up with

$$\hat{I}(x,y,z,s) = \frac{1}{4\pi R} \int_{\tau=R/c_0}^{\infty} \exp(-s\tau) \left(1 - \frac{xc_0\tau}{R^2} \right) \mathrm{d}\tau \tag{33}$$

In view of Lerch's uniqueness theorem of the one-sided Laplace transformation [28, Appendix], the TD counterpart of Eq. (33) immediately follows

$$I(x,y,z,t) = \left(1 - \frac{xc_0 t}{R^2} \right) \frac{\mathrm{H}(t - R/c_0)}{4\pi R} \tag{34}$$

This result is used in Eqs. (17)–(18) to construct the voltage response of a transmission line.

B. Space-time function $J(x,y,z,t)$

The second generic representation to be transformed to the TD has the following form

$$\begin{aligned} \hat{J}(x,y,z,s) &= \frac{c_0}{8\pi^2\mathrm{i}^2} \int_{v=-\mathrm{i}\infty}^{\mathrm{i}\infty} \exp(-svx) \frac{v}{v + c_0^{-1}} \mathrm{d}v \\ &\times \int_{p=-\mathrm{i}\infty}^{\mathrm{i}\infty} \exp\{-s[py + \gamma_0(v,p)z]\} \frac{p\mathrm{d}p}{\gamma_0(v,p)} \end{aligned} \tag{35}$$

for $x, y \in \mathbb{R}$, $\{z \in \mathbb{R}; z > 0\}$, $\{s \in \mathbb{R}; s > 0\}$. Its transformation to the TD follows the procedure closely described in the previous section. In this way, it can be found that

$$J(x,y,z,t) = P(x,y,z,t) \frac{\mathrm{H}(t - R/c_0)}{4\pi R} \tag{36}$$

in which

$$\begin{aligned} P(x,y,z,t) &= (y/d^2 c_0 t)\{xc_0 t - x^2 + c_0^2 t^2 d^2/R^2 \\ &\quad - [R(c_0^2 t^2 - x^2) + c_0 t d^2]/(R + c_0 t)\} \end{aligned} \tag{37}$$

and recall that $d = (y^2 + z^2)^{1/2}$ and $R = (x^2 + d^2)^{1/2}$. The space-time function (36) is used in Eqs. (17)–(18) to construct the voltage response of a transmission line.

C. Space-time function $K(x,y,z,t)$

The last generic integral to be transformed to the TD has the following form

$$\begin{aligned} \hat{K}(x,y,z,s) &= \frac{c_0}{8\pi^2\mathrm{i}^2} \int_{\kappa=-\mathrm{i}\infty}^{\mathrm{i}\infty} \exp(-s\kappa x)\kappa\mathrm{d}\kappa \\ &\times \int_{\sigma=-\mathrm{i}\infty}^{\mathrm{i}\infty} \exp\{-s[\sigma y + \gamma_0(\kappa,\sigma)z]\} \frac{\mathrm{d}\sigma}{\gamma_0(\kappa,\sigma)} \end{aligned} \tag{38}$$

for $x, y \in \mathbb{R}$, $\{z \in \mathbb{R}; z > 0\}$, $\{s \in \mathbb{R}; s > 0\}$. Following the procedure applied in Sec. A again, the TD counterpart of Eq. (38) follows

$$K(x,y,z,t) = \frac{xc_0 t}{R^2} \frac{\mathrm{H}(t - R/c_0)}{4\pi R} \tag{39}$$

This result is used in Eqs. (19)–(20) to construct the voltage response of a transmission line.

ACKNOWLEDGMENT

The first author would like to thank H. A. Lorentz Chair Emeritus Professor Adrianus T. de Hoop for making him acquainted with the applied analytical method.

REFERENCES

[1] I. E. Lager, A. T. De Hoop, and T. Kikkawa, "Pulsed-field wireless interconnects in digital integrated circuits – a time-domain signal transfer and electromagnetic emission analysis," in *6th European Conf. Antennas Propag.*, 2012, pp. 1855–1859.

[2] J. Wu, A. K. Kodi, S. Kaya, A. Louri, and H. Xin, "Monopoles loaded with 3-D-printed dielectrics for future wireless intrachip communications," *IEEE Trans. Antennas Propag.*, vol. 65, no. 12, pp. 6838–6846, 2017.

[3] C. Chen and A. Babakhani, "Wireless synchronization and spatial combining of widely spaced mm-wave arrays in 65-nm CMOS," *IEEE Trans. Microw. Theory Tech.*, vol. 65, no. 11, pp. 4418–4427, 2017.

[4] I. E. Lager, R. B. Staszewski, A. B. Smolders, and D. M. Leenaerts, "Ultra-high data-rate wireless transfer in a saturated spectrum – new paradigms," in *44th European Microw. Conf.*, 2014, pp. 917–920.

[5] H. Aggrawal, P. Chen, M. M. Assefzadeh, B. Jamali, and A. Babakhani, "Gone in a picosecond: Techniques for the generation and detection of picosecond pulses and their applications," *IEEE Micr. Mag.*, vol. 17, no. 12, pp. 24–38, 2016.

[6] D. Pepe, L. Aluigi, and D. Zito, "Sub-100 ps monocycle pulses for 5G UWB communications," in *10th European Conf. Antennas Propag.*, 2016, pp. 1–4.

[7] R. W. P. King, *Transmission-line Theory*, 2nd ed. Dover Publications, Inc., 1965.

[8] C. Taylor, R. Satterwhite, and C. Harrison, "The response of a terminated two-wire transmission line excited by a nonuniform electromagnetic field," *IEEE Trans. Antennas Propag.*, vol. 13, no. 6, pp. 987–989, 1965.

[9] A. K. Agrawal, H. J. Price, and S. H. Gurbaxani, "Transient response of multiconductor transmission lines excited by a nonuniform electromagnetic field," *IEEE Trans. Electromagn. Compat.*, vol. 22, no. 2, pp. 119–129, 1980.

[10] P. Degauque and A. Zeddam, "Remarks on the transmission-line approach to determining the current induced on above-ground cables," *IEEE Trans. Electromagn. Compat.*, vol. 30, no. 1, pp. 77–80, 1988.

[11] F. M. Tesche, "Comparison of the transmission line and scattering models for computing the HEMP response of overhead cables," *IEEE Trans. Electromagn. Compat.*, vol. 34, no. 2, pp. 93–99, 1992.

[12] G. S. Smith, "Analysis of miniature electric field probes with resistive transmission lines," *IEEE Trans. Microw. Theory Tech.*, vol. 29, no. 11, pp. 1213–1224, 1981.

[13] N. W. Damiano, J. Li, C. Zhou, D. E. Brocker, Y. Qin, D. H. Werner, and P. L. Werner, "Simulation and measurement of medium-frequency signals coupling from a line to a loop antenna," *IEEE Trans. Appl. Ind.*, vol. 52, no. 4, pp. 3527–3534, 2016.

[14] M. Leone and H. L. Singer, "On the coupling of an external electromagnetic field to a printed circuit board trace," *IEEE Trans. Electromagn. Compat.*, vol. 41, no. 4, pp. 418–424, 1999.

[15] F. Napolitano, F. Tossani, C. A. Nucci, and F. Rachidi, "On the transmission-line approach for the evaluation of LEMP coupling to multiconductor lines," *IEEE Trans. Power Del.*, vol. 30, no. 2, pp. 861–869, 2015.

[16] R. Olsen and M. Usta, "The excitation of current on an infinite horizontal wire above earth by a vertical electric dipole," *IEEE Trans. Antennas Propag.*, vol. 25, no. 4, pp. 560–565, 1977.

[17] F. Middelstaedt, S. V. Tkachenko, and R. Vick, "Transmission line reflection coefficient including high-frequency effects," *IEEE Trans. Antennas Propag.*, vol. 66, no. 8, pp. 4115–4122, 2018.

[18] N. Ari and W. Blumer, "Analytic formulation of the response of a two-wire transmission line excited by a plane wave," *IEEE Trans. Electromagn. Compat.*, vol. 30, no. 4, pp. 437–448, 1988.

[19] Y. Yao, T. Hirano, K. Okada, J. Hirokawa, and M. Ando, "60 GHz on-chip loop antenna integrated in a 0.18 μm CMOS technology," in *Proc. Int. Symp. Antennas & Propag.*, vol. 2, 2013, pp. 927–929.

[20] I. E. Lager, V. Voogt, and B. J. Kooij, "Pulsed EM field, close-range signal transfer in layered configurations – a time-domain analysis," *IEEE Trans. Antennas Propag.*, vol. 62, no. 5, pp. 2642–2651, 2014.

[21] M. Štumpf, "Pulsed vertical-electric-dipole excited voltages on transmission lines over a perfect ground – a closed-form analytical description," *IEEE Antennas Wireless Propag. Lett.*, vol. 17, no. 9, pp. 1656–1658, Sep. 2018.

[22] M. Štumpf and G. Antonini, "Lightning-induced voltages on transmission lines over a lossy ground – an analytical coupling model based on the Cooray–Rubinstein formula," *IEEE Trans. Electromagn. Compat.*, 2018.

[23] D. Pozar, R. McIntosh, and S. Walker, "The optimum feed voltage for a dipole antenna for pulse radiation," *IEEE Trans. Antennas Propag.*, vol. 31, no. 4, pp. 563–569, 1983.

[24] W. C. Chew, *Waves and Fields in Inhomogeneous Media*. Piscataway, NJ: IEEE Press, 1995.

[25] A. T. De Hoop, "A modification of Cagniard's method for solving seismic pulse problems," *Applied Scientific Research*, vol. B, no. 8, pp. 349–356, 1960.

[26] M. Štumpf, A. T. De Hoop, and G. A. E. Vandenbosch, "Generalized ray theory for time-domain electromagnetic fields in horizontally layered media," *IEEE Trans. Antennas Propag.*, vol. 61, no. 5, pp. 2676–2687, May 2013.

[27] A. T. De Hoop, *Handbook of Radiation and Scattering of Waves*. London, UK: Academic Press, 1995.

[28] M. Štumpf, *Electromagnetic Reciprocity in Antenna Theory*. Hoboken, NJ: IEEE Press–Wiley, 2018.

[29] M. Štumpf and G. Antonini, "Electromagnetic field coupling to a transmission line – a reciprocity-based approach," *IEEE Trans. Electromagn. Compat.*, 2018.

[30] F. Xiao, W. Liu, and Y. Kami, "Analysis of crosstalk between finite-length microstrip lines: FDTD approach and circuit-concept modeling," *IEEE Trans. Electromagn. Compat.*, vol. 43, no. 4, pp. 573–578, 2001.

[31] G. Lupò, C. Petrarca, V. Tucci, and M. Vitelli, "EM fields generated by lightning channels with arbitrary location and slope," *IEEE Trans. Electromagn. Compat.*, vol. 42, no. 1, pp. 39–53, 2000.

[32] M. V. De Hoop and A. T. De Hoop, "Interface reflection of spherical acoustic waves in the first-and second-order rational parabolic approximations and their artifacts," *J. Acoust. Soc. Am.*, vol. 93, no. 1, pp. 22–35, 1993.

Martin Štumpf (M'15) received his Ph.D. degree in electrical engineering from the Brno University of Technology (BUT), Brno, The Czech Republic, in 2011. After his Ph.D. research, he spent a year and a half as a Post-Doctoral Fellow with the ESAT-TELEMIC Division, Katholieke Universiteit Leuven, Leuven, Belgium. He is currently an Associate Professor with the Department of Radioelectronics, BUT. During a three-month period in 2018, he was a Visiting Professor at the UAq EMC Laboratory, University of L'Aquila, Italy. He has authored the books "*Electromagnetic Reciprocity in Antenna Theory*" (Wiley–IEEE Press, 2017), "*Pulsed EM Field Computation in Planar Circuits: The Contour Integral Method*" (CRC Press, 2018), and "*Time-Domain Electromagnetic Reciprocity in Antenna Modeling*" (Wiley–IEEE Press, 2019). His main research interests include modeling of electromagnetic wave phenomena with an emphasis on EMC and antenna engineering.

Giulio Antonini (M'94 - SM'05) received the Laurea degree (*cum laude*) in electrical engineering from the University of L'Aquila, L'Aquila, Italy, in 1994 and the Ph.D. degree in electrical engineering from University of Rome "La Sapienza" in 1998. Since 1998, he has been with the UAq EMC Laboratory, University of L'Aquila, where he is currently a Professor. He has coauthored the book "*Circuit Oriented Electromagnetic Modeling Using the PEEC Techniques*", (Wiley–IEEE Press, 2017). His scientific interests are in the field of computational electromagnetics.

Ioan E. Lager (SM'14) received his MSc-degree in Electrical Engineering (1987) from the "Transilvania" University of Braşov, Braşov, Romania, a PhD-degree in Electrical Engineering (1996) from Delft University of Technology, Delft, the Netherlands, and a second PhD-degree in Electrical Engineering (1998) from the "Transilvania" University of Braşov. He successively occupied several research and academic positions with the "Transilvania" University of Braşov and the Delft University of Technology, where he is currently an Associate Professor. In 1997 he was a Visiting Scientist with Schlumberger-Doll Research, Ridgefield, CT, USA. Dr. Lager has a special interest for bridging the gap between electromagnetic field theory and the design, implementation and physical measurement of radio-frequency front-end architectures. His interests are in applied electromagnetics, especially time-domain propagation and applications, and antenna engineering, with an emphasis on nonperiodic (interleaved) array antenna architectures. He currently investigates effective methods for teaching electromagnetic field theory at (under)graduate-level.